Supplementary Information

Diastereoselective self-assembly of a triple-stranded europium helicate with light modulated chiroptical property

Zhihui Zhang, Yanyan Zhou, Ting Gao, Pengfei Yan, Xiaoyan Zou* and Hongfeng Li*

Key Laboratory of Functional Inorganic Material Chemistry, Ministry of Education, P. R. China; School of Chemistry and Materials Science, Heilongjiang University, Harbin 150080, P. R. China.

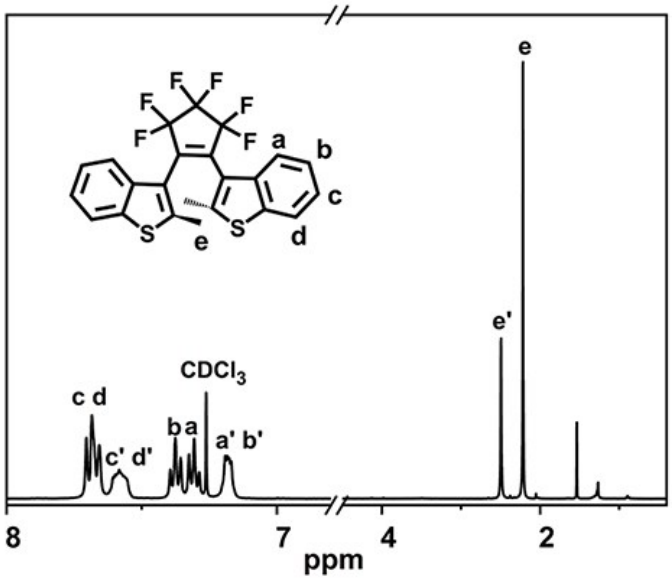

Figure S1. ^{1}H NMR spectrum of **3** in $CDCl_3$.

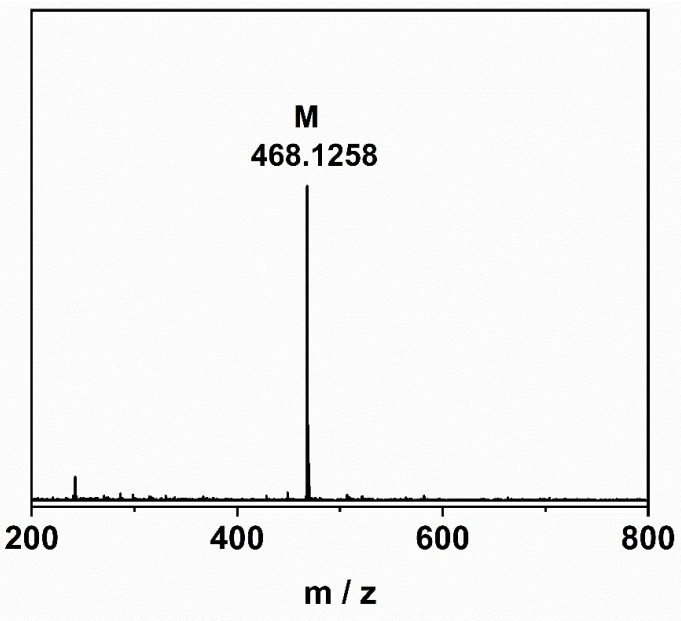

Figure S2. ESI-MS of **3**.

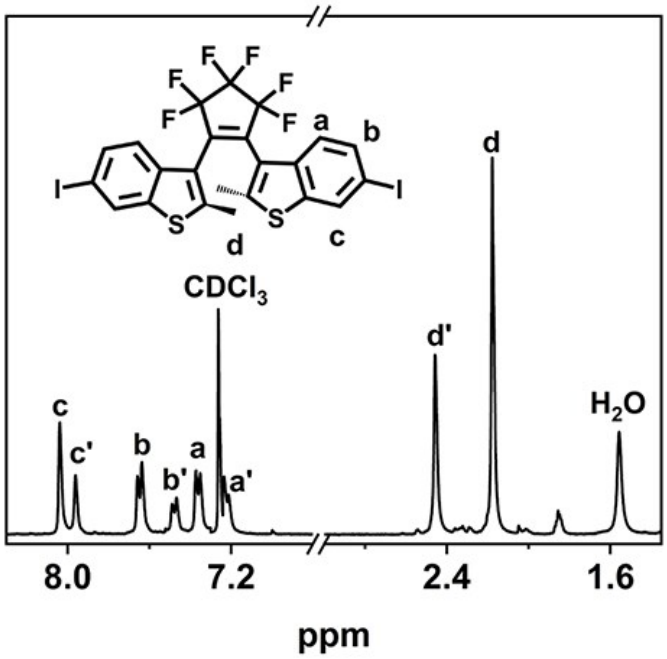

Figure S3. ^{1}H NMR spectrum of **4** in $CDCl_3$.

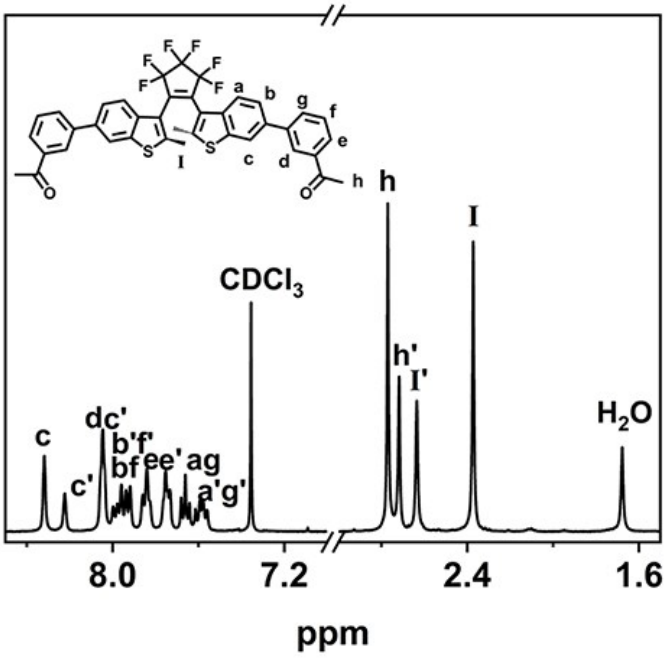

Figure S4. ^{1}H NMR spectrum of **5** in $CDCl_3$.

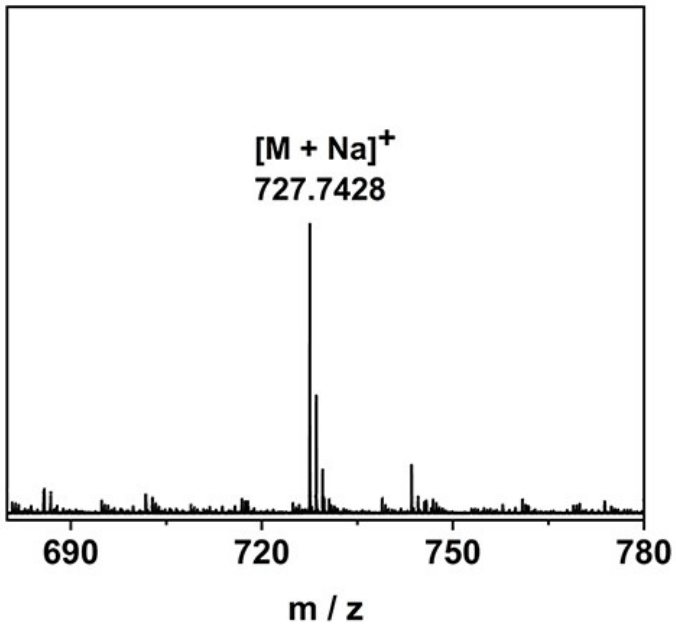

Figure S5. ESI-TOF-MS of **5**.

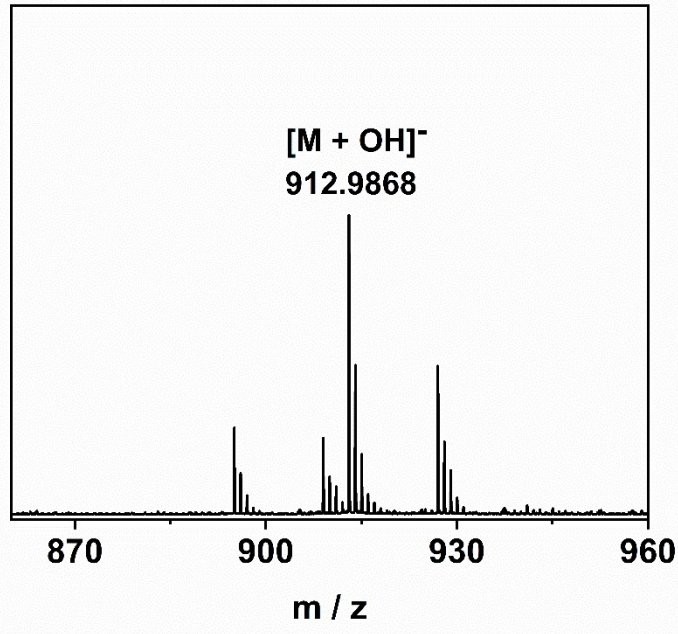

Figure S6. ESI-TOF-MS of **L**.

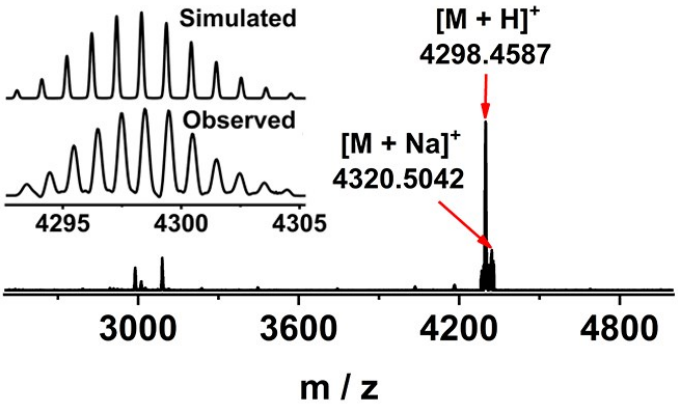

Figure S7. ESI-TOF-MS of Eu_2(o-**L**)$_3$(R-BINAPO)$_2$ (ΔΔ-**1**).

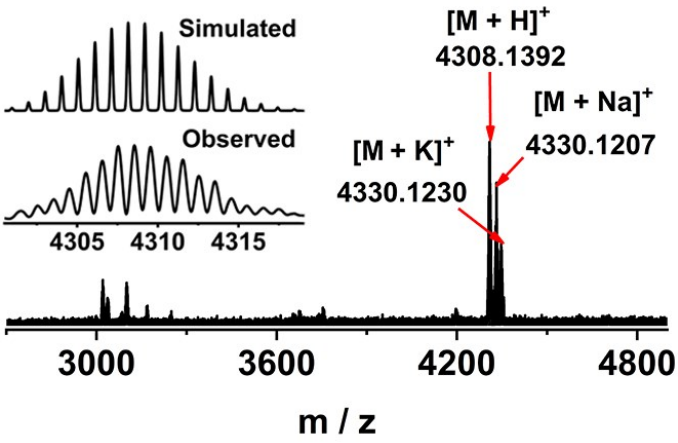

Figure S8. ESI-TOF-MS of Gd_2(o-**L**)$_3$(R-BINAPO)$_2$ (ΔΔ-**1**).

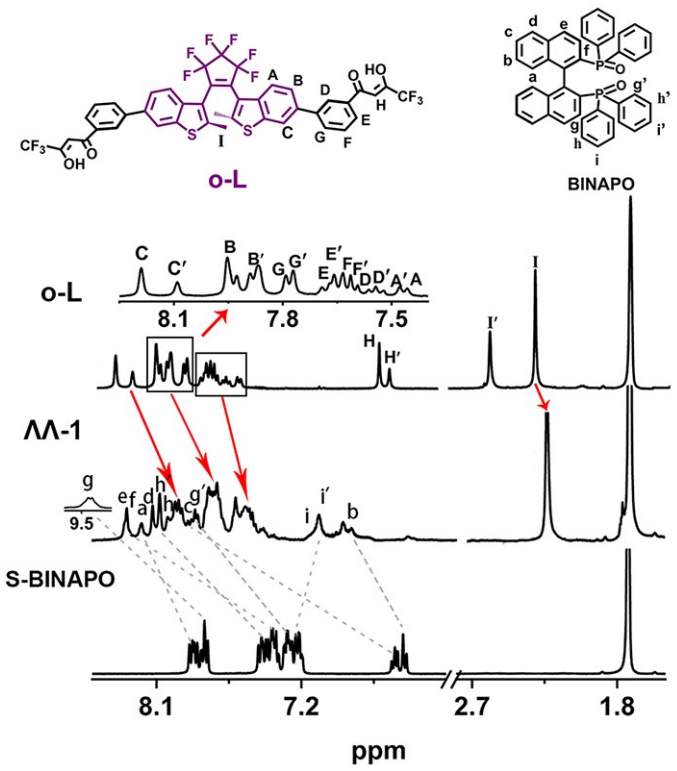

Figure S9. ^{1}H NMR spectra of **L**, S-BINAPO, Eu_2(o-**L**)$_3$(S-BINAPO)$_2$ (ΛΛ-**1**) in THF-d_8.

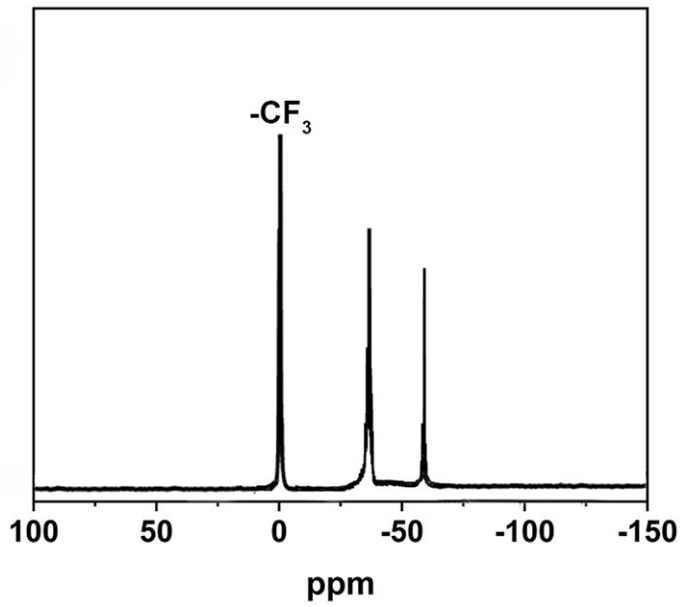

Figure S10. ^{19}F NMR spectrum of Eu_2(o-**L**)$_3$(R-BINAPO)$_2$ (ΔΔ-**1**) in THF-d_8.

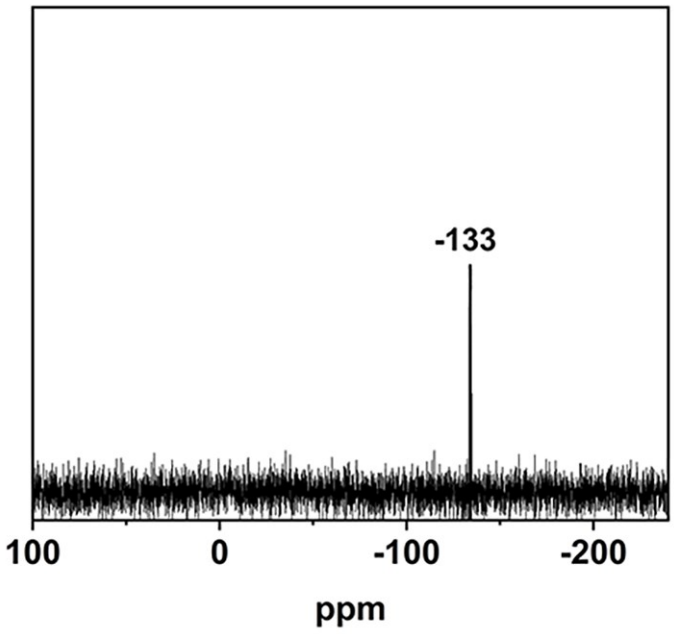

Figure S11. ^{31}P NMR spectrum of Eu_2(o-**L**)$_3$(R-BINAPO)$_2$ (ΔΔ-**1**) in THF-d_8.

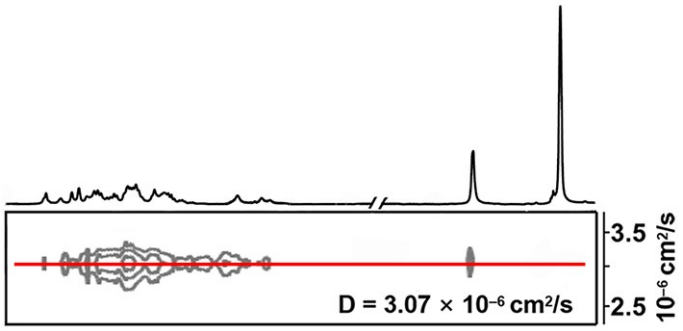

Figure S12. ^{1}H DOSY spectrum of Eu_2(o-**L**)$_3$(S-BINAPO)$_2$ (ΛΛ-**1**) in THF-d_8.

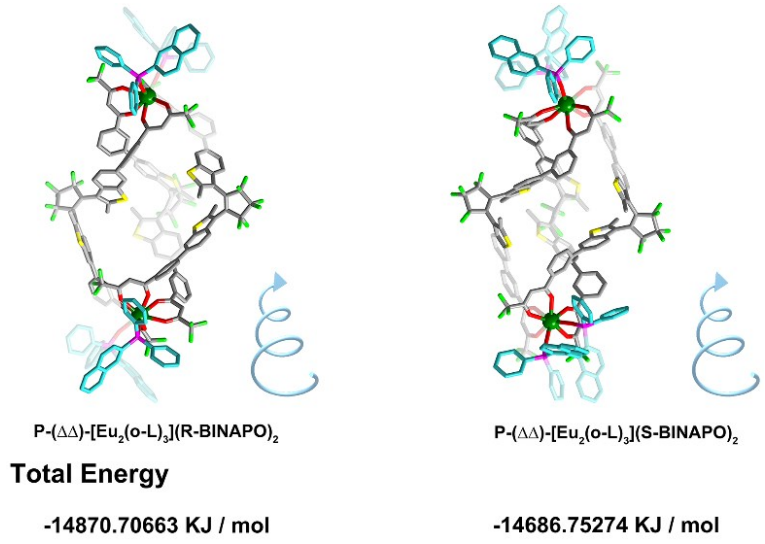

Figure S13. *P* in one helicate based on R-BINAPO and S-BINAPO, and the total energy of each

possible helicate. The molecular mechanic modeling was built by using the MOPAC 2016 program implemented in the LUMPAC 3.0 software with a Sparkle/AM1 model.

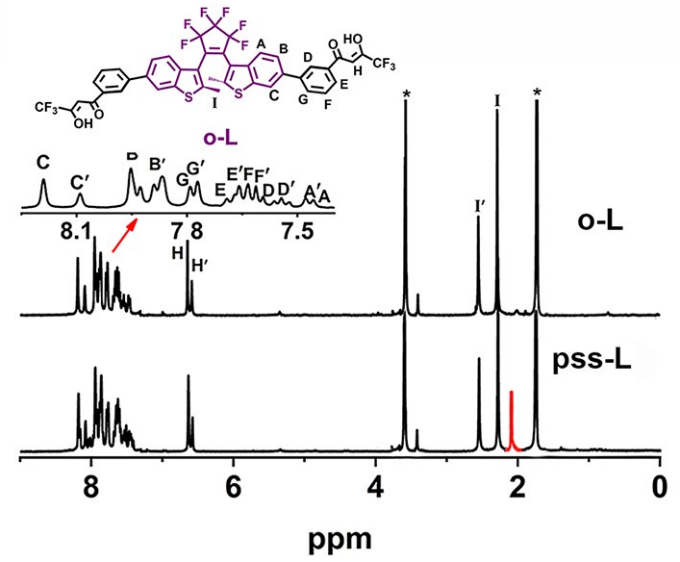

Figure S14. ^{1}H NMR spectra of o-**L** and pss-**L** in THF-d_8.

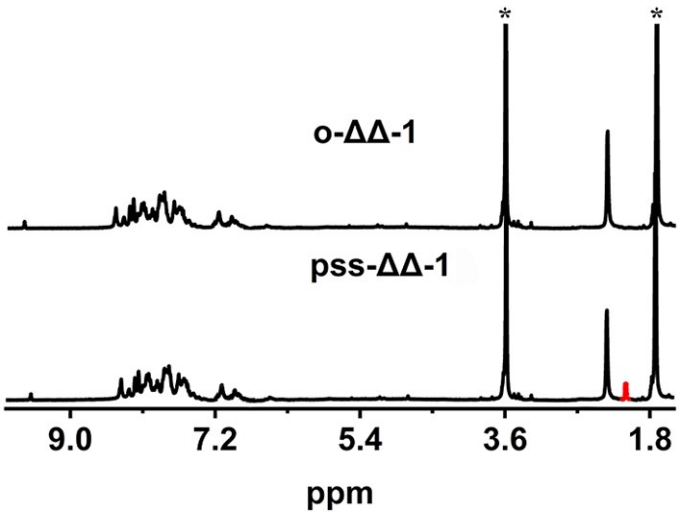

Figure S15. ^{1}H NMR spectra of Eu_2(o-**L**)$_3$(R-BINAPO)$_2$ (o-ΔΔ-**1**) and Eu_2(pss-**L**)$_3$(R-BINAPO)$_2$ (pss-ΔΔ-**1**) in THF-d_8.

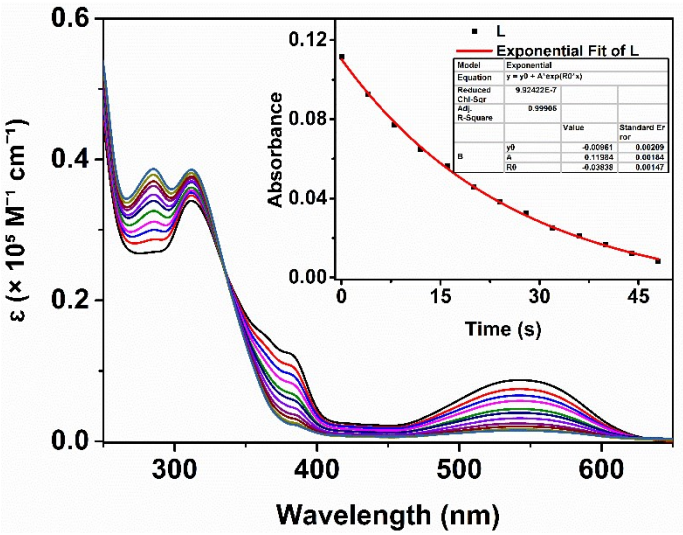

Figure S16. UV/Vis spectra changes of **L** in PSS in THF upon irradiation at 526 nm light (c = 1.0 × 10^{-5} M, $I_{526\ nm}$ = 0.4 × 10^{-3} W/cm^2).

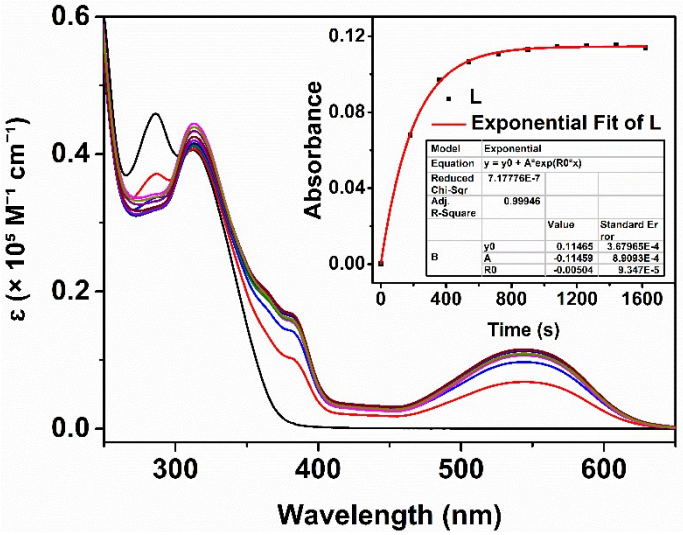

Figure S17. UV/Vis spectra changes of **L** in THF upon irradiation at 275 nm light (c = 1.0 × 10^{-5} M, I_{275} = 1.6 × 10^{-3} W/cm^2).

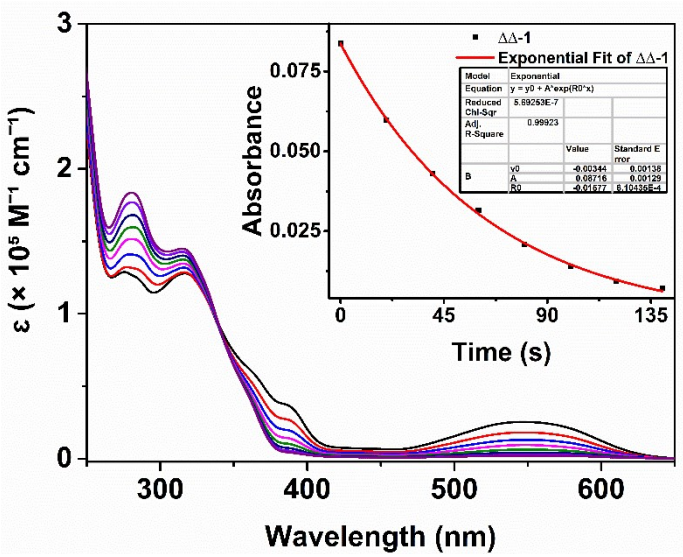

Figure S18. UV/Vis spectra changes of $(Eu_2\mathbf{L}_3)(R\text{-BINAPO})_2$ (ΔΔ-**1**) in PSS in THF upon irradiation at 526 nm light (c = 3.3 × 10^{-6} M, $I_{526\ nm}$ = 0.4 × 10^{-3} W/cm^2).

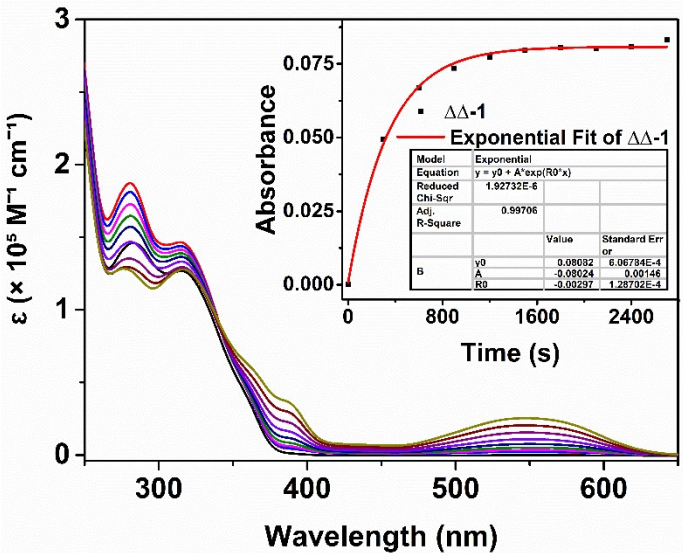

Figure S19. UV/Vis spectra changes of Eu_2(o-**L**)$_3$(R-BINAPO)$_2$ (ΔΔ-**1**) in THF upon irradiation at 275 nm light (c = 3.3 × 10^{-6} M, I_{275} = 1.6 × 10^{-3} W/cm^2).

Table S1. g_{abs} values for $Eu_2\mathbf{L}_3$(R-BINAPO)$_2$ (ΔΔ-**1**) and $Eu_2\mathbf{L}_3$(S-BINAPO)$_2$ (ΛΛ-**1**) after irradiation with UV and visible light

Complexes	g_{abs} ($\times 10^{-4}$)				
	λ = 303 nm	λ = 336 nm	λ = 361nm	λ = 458 nm	λ = 548 nm
o-ΔΔ-**1**	–1.30	–0.69	−1.01	-	-
o-ΛΛ-**1**	1.34	0.67	1.05	-	-
pss-ΔΔ-**1**	−2.28	−0.85	−1.11	−8.24	1.38
pss-ΛΛ-**1**	2.21	0.87	1.09	8.22	−1.35

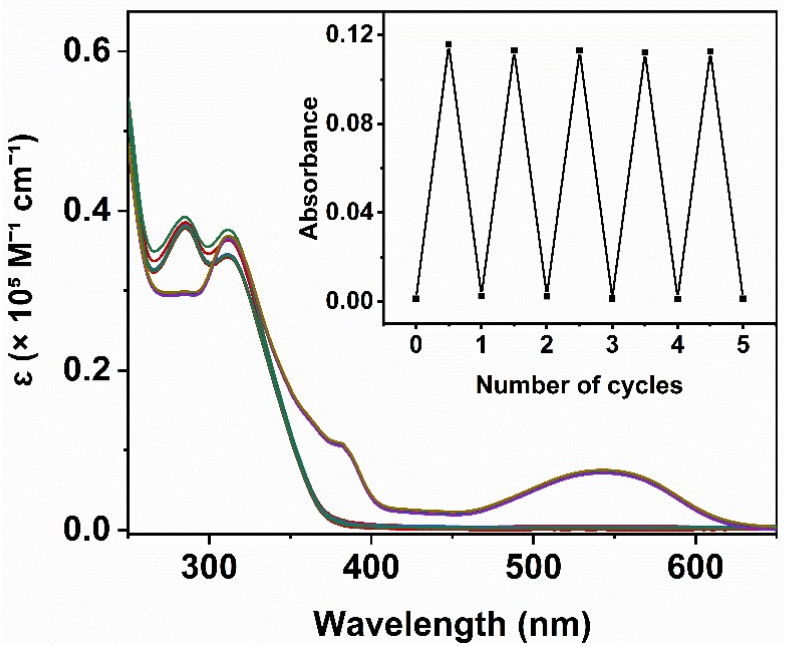

Figure S20. UV/Vis absorbance changes of **L** in THF on alternate excitation at 275 and 526 nm after five cycles at 293 K. *Inset:* The absorbance changes at 545 nm upon repeated alternating UV/vis irradiations.

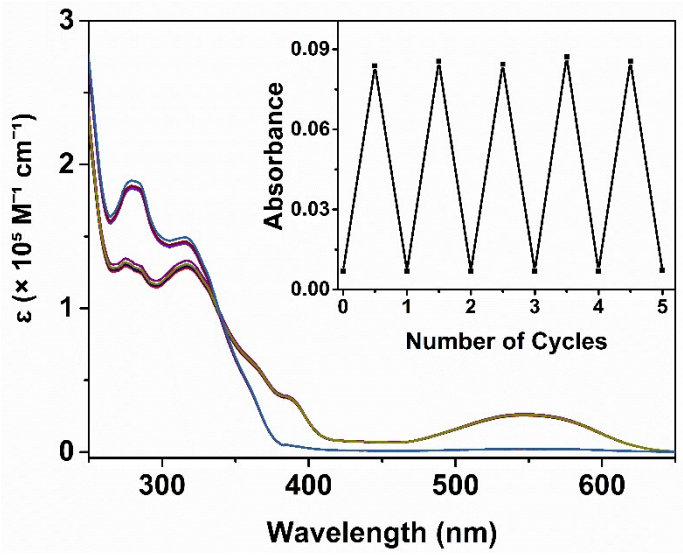

Figure S21. UV/Vis absorbance changes of $(Eu_2\mathbf{L}_3)(R\text{-}BINAPO)_2$ (ΔΔ-**1**) in THF on alternate excitation at 275 and 526 nm after five cycles at 293 K. *Inset:* The absorbance changes at 548 nm upon repeated alternating UV/vis irradiations.

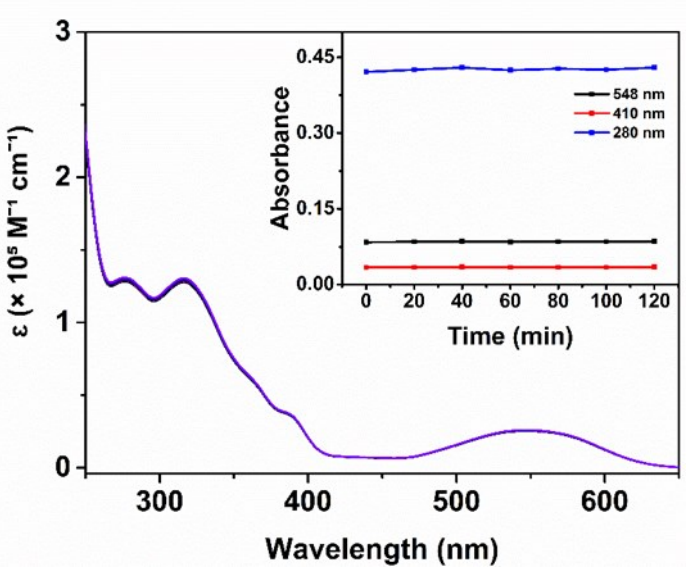

Figure S22. UV/Vis spectra of $(Eu_2\mathbf{L}_3)(R\text{-}BINAPO)_2$ (pss-ΔΔ-**1**) in PSS at different heating times (55 °C for 2 h in THF); no change was observed in shape and intensity, indicating no back reaction to $Eu_2(o\text{-}\mathbf{L})_3(R\text{-}BINAPO)_2$ (o-ΔΔ-**1**). *Insert*: Absorbance changes of the open-ring/ close-ring mixture monitored at 280, 410, and 548 nm.

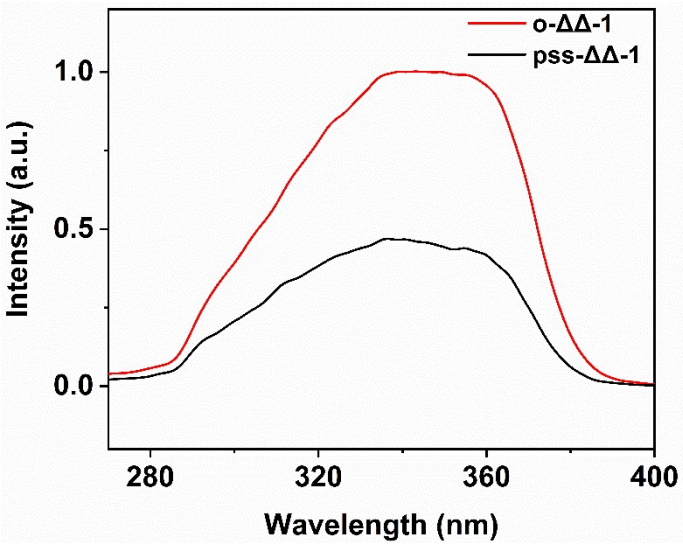

Figure S23. Excitation spectra of Eu_2(o-**L**)$_3$(R-BINAPO)$_2$ (o-ΔΔ-**1**) (red line) and Eu_2(pss-**L**)$_3$ (R-BINAPO)$_2$ (pss-ΔΔ-**1**) (black line) in THF (3.3×10^{-6} M).

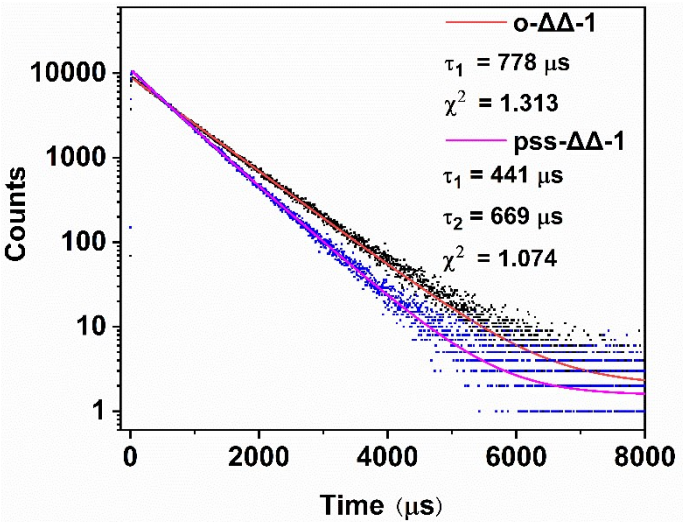

Figure S24. Luminescence decay curves of Eu_2(o-**L**)$_3$(R-BINAPO)$_2$ (o-ΔΔ-**1**) (red line) and Eu_2(pss-**L**)$_3$(R-BINAPO)$_2$ (pss-ΔΔ-**1**) (purple line) in THF monitored at 612 nm.

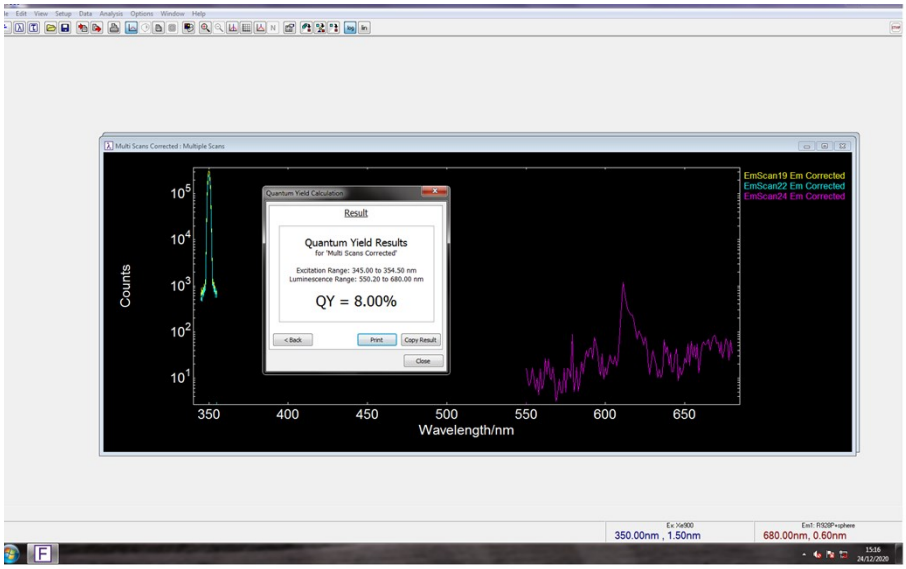

Figure S25. The screenshot of the luminescence quantum yield measurement of Eu_2(o-**L**)$_3$ (R-BINAPO)$_2$ (o-ΔΔ-**1**).

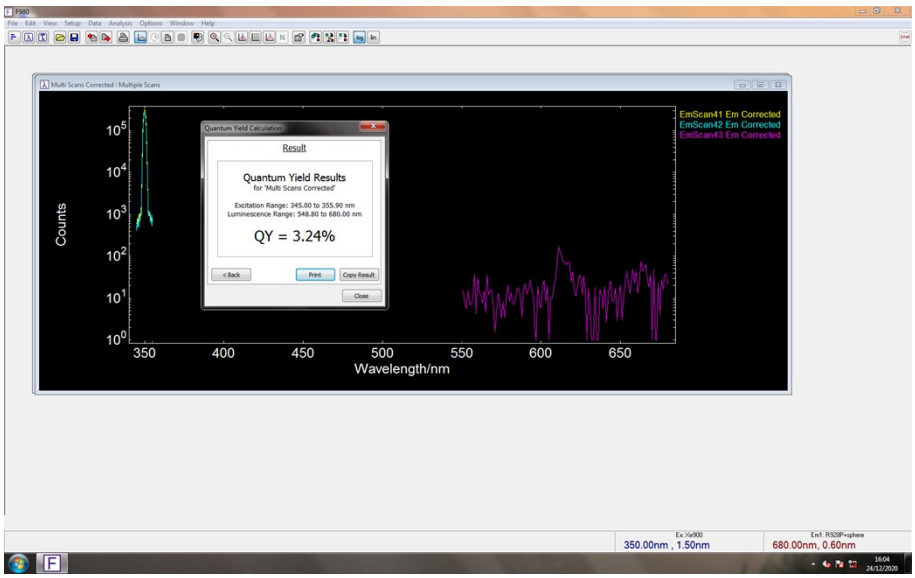

Figure S26. The screenshot of the luminescence quantum yield measurement of Eu_2(pss-**L**)$_3$ (R-BINAPO)$_2$ (pss-ΔΔ-**1**).

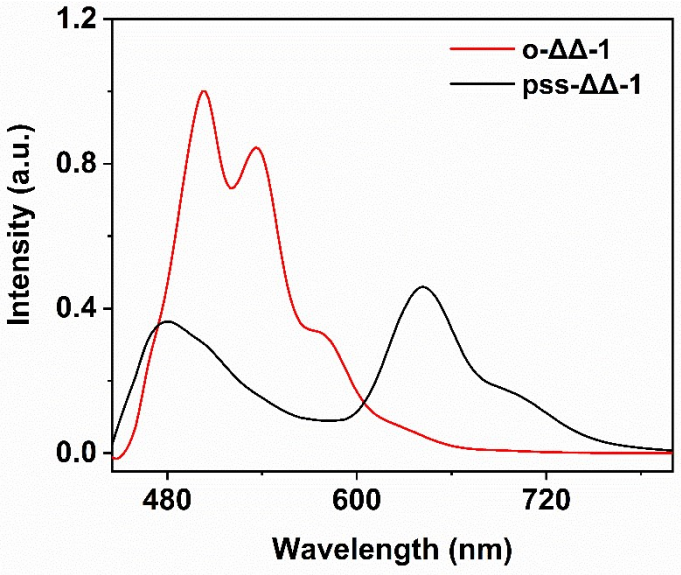

Figure S27. Phosphorescence spectra of Gd_2(o-**L**)$_3$(R-BINAPO)$_2$ (o-ΔΔ-**1**) (red line) and Gd_2(pss-**L**)$_3$(R-BINAPO)$_2$ (pss-ΔΔ-**1**) (black line) at 77 K in THF.

Supplementary Notes

Supplementary Note 1. The cyclization and cycloreversion quantum yields calculation.

The quantum yields of photoisomerization reactions were measured following the reported method (Supplementary Equation 1−7). The kinetics of re-equilibration from an arbitrary initial photostationary state (A_0) to a new phostationary state (A_{pss}) dictated by exposure to light of a given wavelength, is monoexponential (Supplementary Figures S16−S19 and Supplementary Equation 1). The rate constant of equilibration (κ_{eq}) is given by the sum of the two apparent first-order rate constants defining the overall transition and the equilibrium constant (K_{pss}) by their ratio. κ_{ex} is the rate constants for absorption at excitation wavelength. σ_{ex} (cm^2 molecule^{-1}) is the absorption cross-section at excitation wavelength λ_{irr} (nm). ψ_{ex} (photons s^{-1}cm^{-2}) is the photon flux. I (W cm^{-2}) is the intensity of irradiation light, it is 1.6 mW/cm^2 for 275 nm and 0.4 mW/cm^2 for 526 nm. N_A is the Avogadro's constant. α_{pass} is the fractional population of closed form in PSS under 275 nm irradiation and calculated from ^{1}H NMR (Figs. S14 and S15). The concentration for **L** and (Eu_2**L**$_3$)(R/S-BINAPO)$_2$ in THF are 1.0×10^{-5} M and 3.3×10^{-6} M, respectively.

$$A(t) = A_{pss} + (A_0 - A_{pss})\, e^{-\kappa eq\, t} \quad (1)$$

$$\kappa_{eq} = \kappa_{o\rightarrow c} + \kappa_{c\rightarrow o}, \quad (2)$$

$$K_{pss} = [\text{Open form}] / [\text{closed form}] = \kappa_{o\rightarrow c} / \kappa_{c\rightarrow o} \quad (3)$$

$$a_{pss} = K_{pss} / (1 + K_{pss}) = \kappa_{o\rightarrow c} / \kappa_{eq} \quad (4)$$

$$\kappa_{ex} = \sigma_{ex}\, \psi_{ex},\ \sigma_{ex} = (10^3 \ln 10/N_A)\, \varepsilon_{irr},\ \psi_{ex} = 5 \times 10^{15} \lambda_{irr}\, I \quad (5)$$

$$\Phi_{o \to c} = \kappa_{o \to c} / \kappa_{ex,o} \quad (6)$$

$$\Phi_{c \to o} = \kappa_{c \to o} / \kappa_{ex,c} \quad (7)$$

Supplementary Note 2. Computational Details

The ground state geometries of Eu_2(o-**L**)$_3$(R-BINAPO)$_2$ and Eu_2(o-**L**)$_3$(S-BINAPO)$_2$ were optimized by calculations using LUMPAC with a Sparkle/AM1 model implemented in the MOPAC 2016 software. The keywords used in the calculation reported here were AM1, PRECISE, BFGS, GNORM = 0.25, GEO-OK, SCFCRT = 1.D-10 (to increase the SCF convergence criterion) and XYZ (for Cartesian coordinates) (Supplementary Fig. 2 and S15).